DOI: 10.26599/FSHW.2026.9251193

Contents lists available at SciOpen

Food Science and Human Wellness

journal homepage: https://www.sciopen.com/journal/2097-0765

China Food Publishing Co.

Ginseng acidic polysaccharide 15y-GP4 alleviates chronic heart failure by targeting hypoxia-inducible factor-1α and protein phosphatase 6-mediated hypoxia

Xindan Ai[b, 1], Chunbo Zhao[a, 1], Shujie Zhuang[b], Jiongchao Chen[b], Hongkang Xu[b], Minghui Geng[b], Hao Yue[b, *], Weixia Sun[a, *], Yulin Dai[b, *]

[a] *Department of Nephrology, The First Hospital of Jilin University, 130021, Changchun, China*

[b] *Jilin Ginseng Academy, Changchun University of Chinese Medicine, 130117, Changchun, China*

ABSTRACT: Isoprenaline (ISO) can cause chronic heart failure (CHF) by inducing cardiomyocyte apoptosis and oxidative stress. Polysaccharides present in *Panax ginseng C. A. Mey.* (Ginseng) exhibit potent antioxidant and anti-apoptotic properties, improve hypoxic conditions within the body, and mitigate the damage caused by oxidative stress. This study investigated the activity of ginseng polysaccharides (GP) from different harvest years and their mechanisms of action in alleviating CHF by using *in vivo* and *in vitro* experimental validation. In this study, 5-year-old GP (5y-GP) and 15-year-old GP (15y-GP) were obtained via water extraction and alcohol precipitation. Their protective effects against ISO-induced damage in the H9c2 cell line and antioxidant activities were evaluated. Among these, 15y-GP demonstrated strong biological activity. Subsequently, four fractions were eluted from 15y-GP using a DEAE-52 column and the four polysaccharide components were evaluated; of these, component 15y-GP4 exhibited the strongest biological activity. 15y-GP4 was characterized by Fourier-transform infrared and monosaccharide composition analysis, and its preventive effects on ISO-induced CHF were investigated. 15y-GP4 was characterized as an acidic heteropolysaccharide with high glucuronic acid content. It effectively reduced levels of reactive oxygen species, improved mitochondrial function in myocardial cells, and inhibited apoptosis. Furthermore, 15y-GP4 alleviated ISO-induced CHF by downregulating PI3K/AKT/hypoxia-inducible factor-1α (HIF-1α) expression, while upregulating phosphatase 6 regulatory subunit 2 (SAPS2) and protein phosphatase 6 (PP6) catalytic subunit (PPP6C) expression. Immunoprecipitation and co-localization techniques revealed an association between HIF-1α and PP6, with both playing crucial roles in CHF. These results indicate that 15y-GP4 possesses superior bioactivity in preventing CHF, demonstrating broad prospects for the development of CHF applications.

Keywords: Chronic heart failure; ginseng polysaccharides; hypoxia-inducible factor-1α; protein phosphatase 6

1. Introduction

Panax ginseng C. A. Mey. (Ginseng), a valuable industrial crop, has a favorable safety and tolerability profile for the management of heart diseases [1]. In modern clinical practice, it is increasingly used in formulations targeting myocardial infarction, cardiogenic shock, and chronic heart failure (CHF) [2].

[1] These authors contributed equally to this work.
*** Corresponding author.**
yuehao@ccucm.edu.cn, (H. Yue), sunwx@jlu.edu.cn, (W. Sun), daiyl@ccucm.edu.cn, (Y. Dai)

Received 31 December 2025
Received in revised from 26 January 2026
Accepted 12 February 2026

Furthermore, ginseng serves as the primary active component in many effective traditional Chinese medicine (TCM) formulations, such as Shengmaisan, which exhibits significant efficacy against cardiovascular diseases [3]. These attributes underscore the considerable potential of ginseng for the development of natural product-based therapies. Isoprenaline (ISO) is a non-selective β-adrenergic agonist. When injected into animals, it causes myocardial fibrosis, cardiac hypertrophy, and ultimately CHF, which is similar to the CHF caused by atrial fibrillation in humans [4]. Ginseng has been shown to exhibit significant mitigating effects in an ISO-induced CHF model [5]. Ginsenoside Rd improves mitochondrial function through the Ca^{2+} pathway and alleviates CHF [6]. Ginseng polysaccharides (GP), which are one of the main bioactive components of ginseng, exert protective effects on the heart [7]. However, the effects of GP on CHF via hypoxia-inducible factor-1α (HIF-1α) have not been investigated extensively.

CHF, a manifestation of myocardial systolic and dysmetabolic dysfunction, is a serious clinical condition worldwide. In a deteriorating heart, the ability to use oxygen is reduced, and the heart cannot meet its metabolic demands [8]. At this point, pathological changes in energy metabolism occur, which lead to heart failure. Mitochondria play a unique role in ensuring energy supply; therefore, a decline in cardiac function is thought to be directly related to mitochondrial dysfunction [9]. Damaged mitochondria trigger and amplify apoptotic signaling through multiple mechanisms [10]. Specifically, damaged mitochondria with reduced membrane potential cannot convert energetic substances into ATP [11]. In addition, excess calcium is released into the cytoplasm by abnormal mitochondria with highly permeable membranes [12], causing intracellular calcium overload [13]. Furthermore, damaged mitochondria continue to produce reactive oxygen species (ROS), which lead to uncontrolled oxidative stress and cell death through mitochondrial apoptosis [14], thereby affecting normal heart function [15].

HIF-1 is a heterodimeric transcription factor composed of HIF-1α and HIF-1β subunits and is an important regulator of exercise oxygen homeostasis [16]. HIF-1α plays an important role in cardiac pathology. The specific effects of HIF-1α on the heart are linked to the duration of sustained high cardiac levels of HIF-1α. Short-term elevation of HIF-1α expression produces cardioprotective effects through appropriate changes in angiogenesis and cellular metabolism [17]. However, prolonged chronic high expression of HIF-1α further generates large amounts of ROS and promotes apoptosis, which exacerbates myocardial remodeling and may induce CHF [18]. Increased levels of HIF-1α also been reported in the cardiomyocytes of patients with advanced CHF, suggesting that a long-lasting and chronic increase in the transcription of HIF-1α plays a major role in heart deterioration [19]. Recent evidence has demonstrated that the PI3K/AKT signaling pathway, which acts on HIF-1α and plays an instrumental role in cell proliferation and cell survival, is a predominant signaling pathway involved in cardiomyocyte apoptosis [20]. Protein phosphatase 6 (PP6) is a key protein with cardioprotective effects. PP6 is an evolutionarily conserved serine/threonine protein phosphatase essential for embryogenesis in mice. It is a trimetric holoenzyme that consists mainly of phosphatase 6 regulatory subunit 2 (SAPS2) and PP6 catalytic subunit (PPP6C). PP6 is ubiquitously downregulated in cells through a variety of mechanisms including cell cycle progression, DNA

damage, and the inflammatory response [21]. However, the role of PP6 in HIF-1α signaling has not yet been elucidated.

In this study, we investigated the pharmacological effects and mechanisms of GP on CHF induced by ISO, explored the potential role of HIF-1α in cardiomyocytes and tissues during the progression toward CHF, and analyzed for the first time the relationship between PP6 and HIF-1α.

2. Materials and methods

2.1 Reagents and instruments

The following kits were used: Cell Counting Kit-8 (CCK-8) (Beyotime, Shanghai, China), 20,70-dichlorodihydrofluorescein diacetate (DCFH-DA) (Yuanye, Shanghai, China), Annexin V-FITC/propidium iodide (PI) apoptosis detection kit (Beyotime Biotechnology, Shanghai, China), Bicinchoninic acid assay (BCA) protein assay reagent kit (Solarbio, Beijing, China), Sodium dodecyl sulfate polyacrylamide gel electrophoresis (SDS-PAGE) preparation kit, and Electrochemiluminescence (ECL) substrate kit (Biosharp, Beijing, China). Antibodies targeting GADPH, HIF-1α, HIF-1β, PI3K, P-PI3K, AKT, P-AKT, PPP6C, SAPS2, IgG/AP-goat anti-rabbit IgG (H+L) were purchased from Proteintech (Rosemont, IL, USA). The following reagents used for cell culture experiments: Hoechst 33342, PI (Solarbio, Beijing, China), fetal bovine serum (FBS) (Carlsbad, CA, USA), penicillin–streptomycin (P/S) (Carlsbad, CA, USA), Dulbecco's modified Eagle's medium (DMEM) (HyClone, Logan, UT, USA), H9c2 cell line (Pricella Biotechnology Co., Ltd; Wuhan, China), FBS (Gibco BRL, Grand Island, NY, USA), puromycin (Solarbio, Beijing, China), SAPS2-KD and PPP6C-KD plasmid (OBIO Biosciences, Shanghai, China), isoflurane (RWD Life Science Co., Ltd., China). Polyvinylidene fluoride (PVDF) membrane (Merck, Darmstadt, Germany)laser confocal microscope (Nikon, Tokyo, Japan), CarboPac PA-20 anion-exchange column (Thermo Scientific, Shanghai, China), Vevo 3100 system (FujiFilm VisualSonics, Canada), ICS5000$^+$ (Thermo Scientific, Shanghai, China), chromeleon 7.2 CDS (Thermo Scientific), Nicolet iS5 spectrophotometer (Thermo Fisher Scientific, Madison, WI, USA), electrophoresis apparatus (BIO-RAD, Hercules, CA, USA), BL-420s Bio-Functional Experiment System (Techman Software Co., Ltd., Chengdu, China), CO_2 incubator (Thermo, Waltham, MA, USA), GraphPad Prism v.9 software (GraphPad, San Diego, CA, USA), infinite M200 pro multifunctional microplate reader (Tecan, Männedorf, Switzerland) were used for all preparations and analyses.

2.2 Extraction and preparation

Water and alcohol precipitation were used to extract GP from 5- and 15-year-old ginseng to produce 5-year-old ginseng polysaccharides (5y-GP) and 15-year-old ginseng polysaccharides (15y-GP), respectively. First, the ginseng was dried and pulverized to obtain a powder (250 g), which was then mixed with distilled water (1:20 g/mL). The temperature of the extraction unit was adjusted to 100 °C and the mixture was extracted twice with water for 4 h. The suspension was filtered through a gauze cloth to obtain residual liquid. Next the supernatant was reduced to 100 mL using a rotary evaporator, which was then

deproteinized using the Sevag method. Ethanol precipitation was performed to separate the polysaccharide extracts. The extract was mixed with ethanol, and the mixture was allowed to equilibrate for 24 h at 4 °C. After centrifuging at 8000 rpm for 15 min the GP precipitate was taken and dissolved in distilled water, dialyzed for 3 d in ultrapure water, then frozen at -80 °C and freeze-dried to obtain the polysaccharide powder. A schematic representation of the GP extraction process is shown in Figure 1A.

Gradient elution of 15y-GP was performed using cellulose DEAE-52 columns with 0, 0.1, 0.3, and 0.5 mol/L NaCl at a flow rate of 1.0 mL/min. The sulfuric acid/phenol procedure was used to calculate the absorbance at 490 nm for each sample and to draw a chromatographic elution curve. The appropriate fractions were combined, and the isolated GP samples were dialyzed and freeze-dried to obtain four fractions: 15y-GP1, 15y-GP2, 15y-GP3, and 15y-GP4.

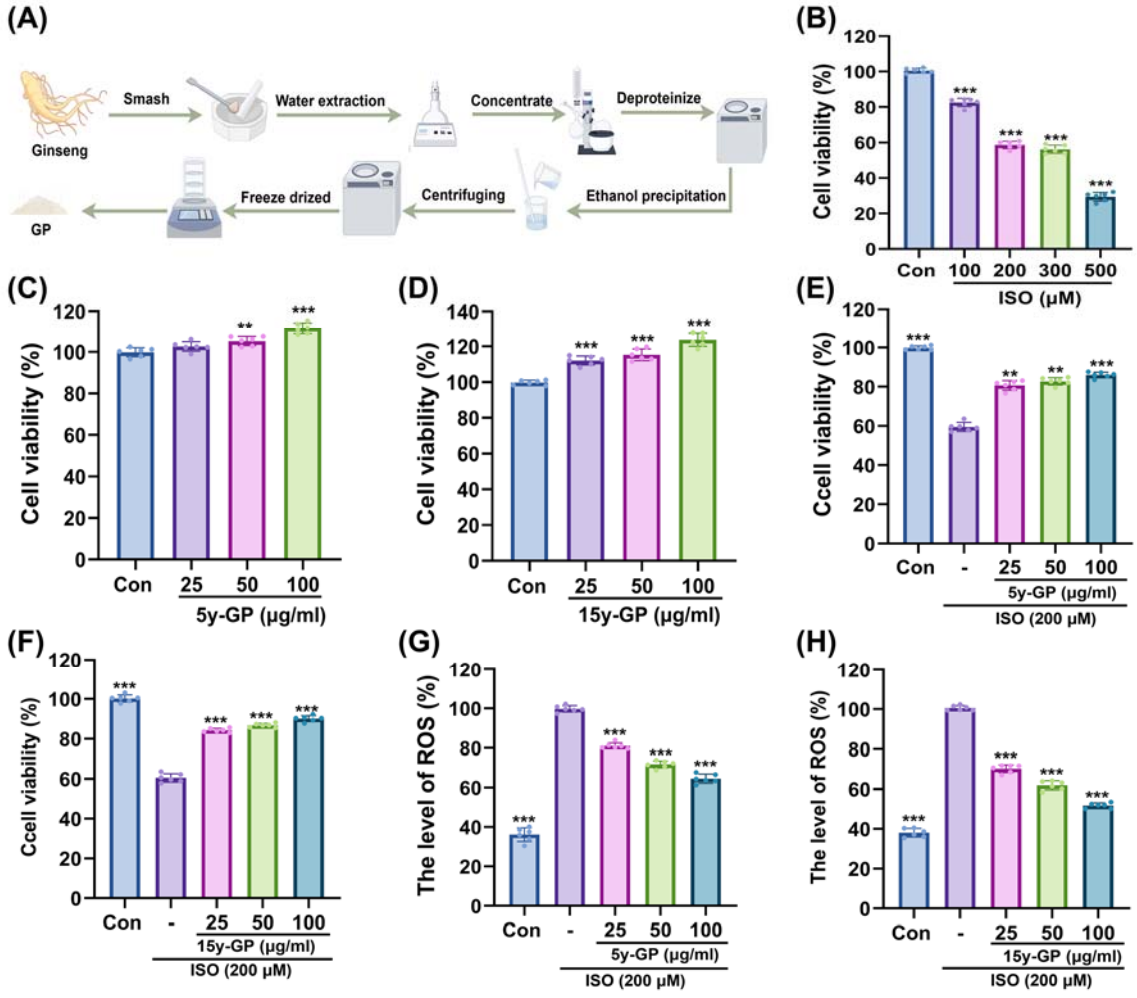

Figure. 1 Protective effect of ginseng polysaccharides (GP) on isoprenaline (ISO)-induced H9c2 cells. (A), GP extraction flow chart. **(B)**, Cell viability of ISO in H9c2 cells. **(C)**, Cell viability of 5-year-old ginseng polysaccharide (5y-GP) in H9c2 cells. **(D)**, Cell viability of 15-year-old ginseng polysaccharide (15y-GP) in H9c2 cells. **(E)**, Cell viability of 5y-GP in ISO-induced H9c2 cells. **(F)**, Cell viability of 15y-GP in ISO-induced H9c2 cells. **(G)**, Detection of 5y-GP in ISO-induced H9c2 cells reactive oxygen species (ROS) level. **(H)**, Detection of 15y-GP in ISO-induced H9c2 cells ROS level. Data are represented as mean ± standard deviation (SD), n=6; *$P < 0.05$, **$P < 0.01$ and ***$P < 0.001$ vs. ISO.

2.3 Monosaccharide composition analysis

Approximately 5 mg of the sample was hydrolyzed with trifluoroacetic acid (2 mol/L) at 121 °C for 2 h in a tightly closed container. The samples were washed with methanol and blow-dried, and the

washing/drying process was repeated three times. Demineralized water was added to the residue, and the solution was filtered through a 0.22 μm microporous filter sheet. The sample extracts were analyzed using high-performance anion-exchange chromatography (HPAEC) on a CarboPac PA-20 anion-exchange column (0.5 mL/min flow rate; 5 μL injection volume) using a pulsed amperometric detector. A three-component solvent system was used consisting of solvents A (ddH_2O), B (0.1 mol/L NaOH), and C (0.1 mol/L NaOH and 0.2 mol/L NaAc), in a gradient program with volume ratios of solutions A, B, and C of 95:5:0 at 0 min, 85:5:10 at 26 min, 85:5:10 at 42 min, 60:0:40 at 42.1 min, 60:40:0 at 52 min, 95:5:0 at 52.1 min, and 95:5:0 at 60 min. Data were captured using an ICS5000$^+$ and processed using the Chromeleon 7.2 CDS. The quantified data were then exported to Excel and organized in tabular form.

2.4 Fourier-transform infrared analysis

A Nicolet iS5 spectrophotometer was employed to record the Fourier-transform infrared (FT-IR) spectrum of the samples in the wavelength range of 400–4000 cm^{-1} using the KBr disc procedure.

2.5 Cell culture

H9c2 cells were cultured in DMEM supplemented with 10% fetal bovine serum (FBS) and 1% penicillin/streptomycin. Cells were cultured at 37 °C in a humidified incubator with 5% CO_2.

2.6 SAPS2 and PPP6C knockdown

Cell transfection was performed according to the manufacturer's instructions to generate SAPS2-knockdown (KD) and PPP6C-KD cell lines. SAPS2-KD and PPP6C-KD lentivirus suspensions were used to infect H9c2 cells, which were then cultured. Identification and selection of cells that were successfully infected was achieved using 1 μg/mL puromycin screening and fluorescence microscopy.

2.7 Screening of ISO dose on H9c2 cells

To obtain the optimum dose of ISO, H9c2 cells were exposed to with different doses (100, 200, 300, and 500 μmol/L) of ISO. A 96-well plate (1×10^4 cells/wells) was seeded with H9c2 cells and incubated at 37 °C in a 5% CO_2 incubator overnight. Different doses of ISO were then added to each well, with the exception of the control (Con), and cell viability was determined after incubation for a further 24 h. For follow-up experiments, the ISO dose that led to 60% cell survival was used.

2.8 Determination of cytotoxicity of ginseng crude polysaccharides in H9c2 cells

To measure the viability of H9c2 cells after treatment with 5y-GP and 15y-GP, the CCK-8 assay was performed. H9c2 cells were seeded (1×10^4 cells/well) in a 96-well plate using DMEM (10% FBS, 1% P/S) and incubated overnight at 37 °C in a 5% CO_2 incubator. The cells were treated with prepared concentrations of 5y-GP (25, 50, and 100 μg/mL) and 15y-GP (25, 50, and 100 μg/mL) and then incubated for 24 h. CCK-8 (10 μL) was then dispensed into each well and after a 1 h incubation in the dark, the absorbance was measured at 450 nm. The selection of 100 μg/mL as a concentration for testing was motivated by previous reports of anti-oxidation effects of GP in H9c2.

2.9 Determination of cytotoxicity and intracellular ROS of ginseng crude polysaccharides in ISO-induced H9c2 cells

Ninety-six-well plates (1×10^4 cells/wells) were seeded with H9c2 cells and treated with 5y-GP (25, 50, and 100 μg/mL) and 15y-GP (25, 50, and 100 μg/mL), respectively. After incubation for 1 h, the cells were treated with ISO (200 μmol/L), and then the cell viability was measured, and the DCFH-DA method was conducted to measure ROS production.

2.10 Determination of cytotoxicity and intracellular ROS of 15y-GP ginseng purified polysaccharides in ISO-induced H9c2 cell

Ninety-six-well plates (1×10^4 cells/wells) were seeded with H9c2 cells and treated with 15y-GP1, 15y-GP2, 15y-GP3, and 15y-GP4 (25, 50, and 100 μg/mL). The cells were incubated for 1 h and then treated with ISO (200 μmol/L). Cell viability was investigated, and ROS formation was measured using the DCFH-DA method.

2.11 Determining cell viability and intracellular ROS with a HIF-1α activator and inhibitor in H9c2 cells

The phosphorylation of the eukaryotic translation initiation factor 4E binding protein 1 and p70 S6 kinase (important regulators of HIF-1α production) are suppressed by KC7F2. Hydroxylated HIF-1 interaction with pVHL is directly inhibited with cobalt chloride ($CoCl_2$) to stabilize HIF-1α [22]. H9c2 cells were also treated with 10 μmol/L KC7F2 (HIF-1α inhibitor) and 100 μmol/L $CoCl_2$ (HIF-1α activator) after adding 15y-GP4. The cells were incubated for 1 h and then treated with ISO (200 μmol/L). Cell viability was assessed, and DCFH-DA was performed to quantify ROS production.

2.12 Hoechst 33342 and PI fluorescent staining

A 6-well plate was seeded with H9c2 cells. When the cell density reached 80%, defined concentrations of 15y-GP4, KC7F2, and $CoCl_2$ were added to the plate. After a 1 h incubation, ISO (200 μmol/L) was added. After a further 24 h incubation, the cells were washed twice with phosphate-buffered saline (PBS) and the PBS was discarded. Hoechst 33342 and PI were added to the cells, and the mixtures were incubated for 20 min in the dark. A fluorescence microscope was used to visualize the cells.

2.13 Detection of ROS

After treatment of H9c2 cells, the 6-well plates were incubated at 37 °C for 20 min with DCFH-DA stain (2 mL). Serum-free medium was added, and the cells were washed three times. The cells were then visualized using a fluorescence microscope.

2.14 Measurement of calcium concentration with Fluo-4 AM

Following treatment of the H9c2 cells, Fluo-4 AM stock solution was diluted with PBS to give a working solution of 5 μmol/L, which was used for the assay. The growth medium was removed and an appropriate volume of Fluo-4 AM working solution was added to the wells, and the plate was then incubated at 37 °C for 30 min. After excess dye was removed, the cells were washed three times with Hanks' balanced

salt solution (HBSS) to remove residual staining before being covered with HBSS. The cells were further incubated at 37 °C for 30 min and observed by fluorescence microscopy.

2.15 JC-1 staining

Following treatment of H9c2 cells, JC-1 stain working solution (1 mL) was added, and the mixture was incubated for 20 min at 37 °C in an incubator. The supernatant was aspirated and the cells were washed twice with JC-1 staining buffer. JC-1 agglutination in normal mitochondria produces red fluorescence, whereas in diseased mitochondria, monomers produce green fluorescence.

2.16 Flow cytometry analysis

A 6-well plate (1×10^6 cells/well) was inoculated with H9c2 cells and treated with a defined concentration of 15y-GP4, KC7F2, $CoCl_2$, and ISO, and incubated for 24 h at 37 °C. Following digestion with EDTA-free trypsin, the cell precipitates were collected by centrifugation, as described previously, washed with pre-cooled PBS, and the cells were resuspended in 1 × Binding Buffer (500 μL). A total of 5 μL Annexin V-FITC and 5 μL PI were then added and the mixture was incubated for 20 min in the dark at room temperature. Cell detection was performed within 1 h by flow cytometry.

2.17 Western blotting and co-immunoprecipitation

RIPA buffer was used to isolate total proteins from mouse tissues and cell culture samples. Protein levels were measured using the BCA assay. Equivalent volumes of protein were loaded and separated by electrophoresis using SDS-PAGE. The samples were then transferred to PVDF membranes. The membranes were blocked with 5% skim milk at ambient temperature and incubated with primary antibodies at 4 °C overnight. The membranes were then washed again before incubation with secondary antibodies for 3 h at room temperature. The bands were detected using an ECL system. The band intensity was quantified by the mean gray values using ImageJ software.

For co-immunoprecipitation (Co-IP) studies, magnetic beads were incubated with the target antibodies for 1 h, and TBS was used to wash the mixture. Magnetic beads were attached to the protein lysate and incubated for 2 h at ambient temperature. After centrifugation, the supernatant was discarded. The mixture of magnetic beads was washed with lysate containing the inhibitor and buffer containing SDS was added, and then heated at 95 °C for 5 min. The samples were subjected to western blotting analysis.

2.18 Co-localization analysis

H9c2 cells were prepared as cell-crawling slices, covered with 3% BSA and incubated for 30 min at ambient temperature. Subsequent removal of the blocking solution was undertaken and HIF-1α antibody and cells prepared in the relevant proportions were then incubated overnight at 4 °C in a humidified box. The slides were then washed three times with PBS on a decolorizing shaker. Each washing cycle lasted for 5 min. The corresponding horseradish peroxidase-labelled secondary antibody was added dropwise to the circle after the slides were shaken dry and incubated for 50 min at ambient temperature. The slides were then washed three times with PBS for 5 min each. The decolorization procedure was performed using a

decolorization shaker where the slides were then shaken and then dried. TSA was then added dropwise, and the slides were incubated for 10 min at room temperature in the dark, after which the slides were placed in TBST and washed three times for 5 min each on a decolorizing shaker. in a repair box filled with antigen repair buffer and heated in a microwave oven. The prepared PPP6C antibody was added dropwise, and the slides were incubated overnight at 4 °C in a humidity box. The slides were stripped by washing three times in PBS for 5 min each on a decolorization shaker. After the slides were shaken dry, the corresponding fluorescent secondary antibody was added dropwise, and the slides were incubated for 50 min at ambient temperature in the dark. After incubation, the slides were washed thrice in PBS for 5 min each on a decolorization shaker. After the slides were shaken dry, the DAPI staining solution was added dropwise, and the slides were incubated for 10 min at room temperature in the dark. The slides were washed three times in PBS for 5 min each on a decolorization shaker. After the slides were shaken dry, the spontaneous fluorescence quencher B was added to the circles and incubated for 5 min, and an anti-fluorescence quenching sealant was applied. Images were acquired using a confocal laser microscope.

2.19 Animal experiments

Male C57BL/6J mice (6 weeks old) were acquired from the Laboratory Animal Center of Changsheng Biotechnology Co., Ltd. (Shenyang, China). The subjects were provided with unrestricted access to water and food and housed under controlled conditions to ensure the absence of specific pathogens. The effects of age and sex of C57BL/6J mice on the experimental results were reduced by using mice that were matched with factors inherent for the purpose of this study. The implementation of all guidelines conformed to the principles outlined in the Guide for the Care and Use of Laboratory Animals, as established by the National Research Council, and were approved by the Animal Ethics Committee of Changchun University of Chinese Medicine (approved ID: 2025374). The β-AR antagonist propranolol (PRO) was used as a positive control drug [23].

The mice were divided into five groups: control (Con), ISO, PRO, 15y-GP4 prophylactic medication (15y-GP4[PM]), and 15y-GP4 therapeutic medication (15y-GP4[TM]). ISO (30 mg/kg) was injected intraperitoneally once daily for four weeks, PRO was injected intraperitoneally at a single dose of 10 mg/kg, and 15y-GP4 was administered at 100 mg/kg by gavage. The same volume of saline was injected intraperitoneally for four weeks in the Con group.

The focus of the present study was to investigate the role played by HIF-1α in the alleviation of CHF by 15y-GP4. The mice were divided into five groups: Con, ISO, 15y-GP4(PM), 15y-GP4(PM)+KC7F2, and 15y-GP4(PM)+$CoCl_2$. The Con, ISO, and 15y-GP4(PM) groups were administered dosages as described above; the 15y-GP4(PM)+KC7F2 and 15y-GP4(PM)+$CoCl_2$ groups were treated with 15y-GP4, and then KC7F2 (10 mg/kg) or $CoCl_2$ (1 mg/kg) solutions were injected intraperitoneally [24]. After receiving the interventions for four weeks, the mice were used for subsequent measurements.

2.20 Echocardiography and electrocardiograph measurements

Inhaled 3% isoflurane was used to anesthetize mice. M-mode- and B-mode ultrasonographic measurements were recorded from a parametric long-axis view. Measurements were conducted using a Vevo 3100 system and an MX-250 probe. Echocardiography (ECG) yielded several parameters that were used to assess cardiac function. These parameters included left ventricular internal dimensions during systole (LVIDs) and diastole (LVIDd), ejection fraction (EF), and fractional shortening (FS). ECG was performed using a standard II lead electrocardiogram. Electrodes with needles were then inserted into the subcutaneous tissue of the paws of the anesthetized mice. The present study used the BL-420s Bio-Functional Experiment System to continuously record heart signals. This investigation focused on analyzing the QRS segment alterations.

2.21 Collection of heart tissue and mice serum

All mice were euthanized after ECG, and blood samples were collected. Serum was isolated and stored at -80 °C. After blood collection, the heart tissues were carefully excised. The hearts were then washed with pre-cooled saline and dried using filter paper. The cells were fixed in 4% paraformaldehyde. Some hearts were stored at -80 °C.

2.22 Serum biochemical analysis

The levels of NT-BNP and HIF-1α in the supernatants were analyzed by ELISA in accordance with the manufacturer's instructions. Serum was collected, and the concentrations of lactate dehydrogenase (LDH), malondialdehyde (MDA), free fatty acids (FFA), and creatine kinase (CK) were measured using LDH, MDA, FFA, and CK assay kits, respectively, using a microplate reader.

2.23 Hematoxylin and eosin and Picro Sirius red staining

The heart muscle tissue was preserved in 4% paraformaldehyde. The specimen was embedded in paraffin, after which it was sliced into sections measuring 5 μm. Hematoxylin and eosin (H&E) and Picro Sirius red staining were performed to assess histopathological changes and collagen deposition, respectively.

2.24 Statistical analysis

Data analysis was conducted using GraphPad Prism v.9 software. Means are presented as mean ± standard deviation (SD). One-way analysis of variance (ANOVA) was used to compare normally distributed data and to determine statistically significant differences between groups. Statistical significance was set at $*p < 0.05$, $**p < 0.01$, $***p < 0.001$.

3. Results

3.1 Effects of ginseng maturity on the crude polysaccharide composition and activity in ISO-induced H9c2 cells

The active components and pharmacological activities of ginseng vary according to the years of growth. To compare differences in activity of GP from ginseng samples of different ages, 5-year-old ginseng and 15-year-old ginseng samples were analyzed. ISO was used to construct an H9c2 *in vitro* myocardial

injury model. An ISO concentration of 200 μmol/L was identified as the optimal concentration for the ensuing experiments based on the cell survival rate shown in Figure 1B. Interestingly, in the sample toxicity screening experiments, both 15- and 5-year-old ginseng extracts were beneficial to H9c2 cardiomyocytes (Figure 1C, D). The cytoprotective and antioxidant activities of 15-year-old ginseng and 5-year-old ginseng were compared (Figure 1E-H). The activity of 15-year-old ginseng was superior to that of 5-year-old ginseng. Therefore, 15y-GP was selected for subsequent isolation, purification, and activity assays.

3.2 Chemical components and monosaccharide composition analysis of 15y-GP1, 15y-GP2, 15y-GP3, and 15y-GP4

The elution profile of 15y-GP is shown in Figure 2A. The results of the monosaccharide composition analysis of the polysaccharide samples were compared with those of monosaccharide standards (Figure 2B–F). Table 1 shows the yields and monosaccharide compositions of the four samples collected from 15y-GP using DEAE-52. The results reveal different compositions of 15y-GP1 (Ara, Gal, and GLC), 15y-GP2 (Rha, Ara, Gal, Glc, Gal-UA, and Glc-UA), 15y-GP3 (Fuc, Rha, Ara, Gal, Glc, Xyl, Gal-UA, and Glc-UA) and 15y-GP4 (Fuc, Rha, Ara, Gal, Glc, Xyl, Man, Gal-UA, and Glc-UA) were obtained. Glc was the major monosaccharide in 15y-GP, and the highest Gal-UA content was observed in 15y-GP4.

Table 1 Yield and monosaccharide composition of collected samples obtained from 15y-GP by DEAE-52.

Sample	Eluate	Yield (%)	Monosaccharide composition (%)								
			Fuc	Rha	Ara	Gal	Glc	Xyl	Man	Gal-UA	Glc-UA
15y-GP1	0 mM Nacl	31.11	-	-	0.30	1.70	98.00	-	-	-	-
15y-GP2	100 mM Nacl	20.22	-	1.49	4.32	4.63	86.07	-	-	3.07	0.42
15y-GP3	300 mM Nacl	31.33	0.80	1.42	4.53	6.32	82.45	0.33	-	3.57	0.58
15y-GP4	500 mM Nacl	9.67	1.15	1.76	6.94	9.84	75.50	0.59	0.76	3.76	0.70

3.3 FT-IR analyses of 15y-GP1, 15y-GP2, 15y-GP3, and 15y-GP4

As shown in Figure 2G, the OH stretching vibration of each sample showed broad and strong stretching peaks at 3450 cm^{-1}, indicating the presence of OH. The absorption peaks at 2930 cm^{-1} indicated of the C-H bond, the absorption peaks at approximately 1630 cm^{-1} are assigned to the asymmetric stretching vibration of the carbonyl group, and the absorption peaks at approximately 1400 cm^{-1} arose from the vibrations of the C-H bond. The strong absorption peak at 1079 cm^{-1} indicated the presence of pyranose units among the four sugars; the absorption peaks around 850 cm^{-1} was identified as the α-D-pyranose glucose conformation.

3.4 Effects of different polysaccharides isolated from 15y-GP on ISO-induced H9c2 cells

The activities of the four fractional polysaccharides were determined after DEAE isolation and purification. In the sample toxicity screening assay, none of the four concentrations of 15y-GP1, 15y-GP2, 15y-GP3, or 15y-GP4 tested was significantly toxic to H9c2 cells. The survival and ROS scavenging ability of ISO-treated H9C2 cells was examined: 15y-GP4 had stronger antioxidant activity and cardiomyocyte

protection than 15y-GP1, 15y-GP2, and 15y-GP3 (Figure 2H–J). Thus, 15y-GP4 was selected for subsequent experiments.

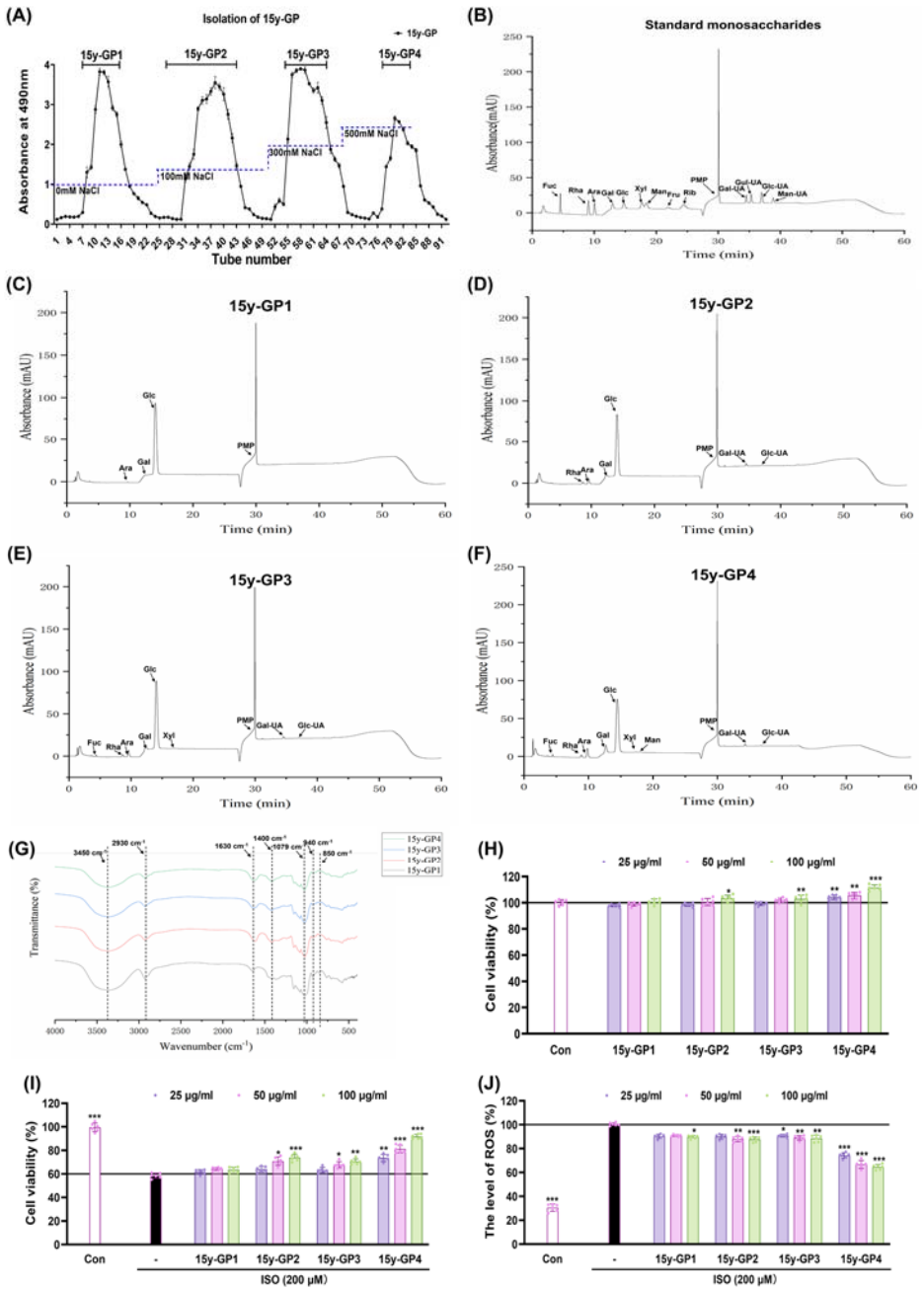

Figure. 2 Characterization and activity analysis of 15y-GP. (A), Elution profile of 15y-GP. **(B)**, chromatogram of standard monosaccharides. **(C)**, chromatogram of 15y-GP1. **(D)**, chromatogram of 15y-GP2. **(E)**, chromatogram of 15y-GP3. **(F)**, chromatogram of 15y-GP4. **(G)**, Fourier-transform infrared (FT-IR) spectra of 15y-GP1, 15y-GP2, 15y-GP3 and 15y-GP4. **(H)**, Cell viability of 15y-GP1, 15y-GP2, 15y-GP3 and 15y-GP4 in H9c2 cells. **(I)**, Cell viability of 15y-GP1, 15y-GP2, 15y-GP3, and 15y-GP4 in ISO-induced H9c2 cells. **(J)**, Detection of 15y-GP1, 15y-GP2, 15y-GP3, and 15y-GP4 in ISO-induced H9c2 cells ROS level. Data are represented as mean ± SD, n=6; *$P < 0.05$, **$P < 0.01$ and ***$P < 0.001$ vs. ISO.

3.5 15y-GP4 protected against ISO-induced apoptosis in H9c2 cells

To assess whether HIF-1α was involved in 15y-GP4-protection against ISO-induced effects in H9c2 cells, the HIF-1α inhibitor KC7F2 and activator $CoCl_2$ were used to regulate HIF-1α expression. The antioxidant activity and H9c2 cytoprotective effects of 15y-GP4 were significantly enhanced by the addition of KC7F2 compared with effects observed when HIF-1α expression was not suppressed, whereas the

addition of $CoCl_2$ significantly weakened the antioxidant activity and the H9c2 cytoprotective effects of 15y-GP4 (Figure 3A,B). The present study supports the hypothesis that HIF-1α is a pivotal protein in myocardial injury caused by ISO. Apoptosis in H9c2 cells was assessed using flow cytometry and Hoechst 33342 PI staining. Hoechst 33342 and PI staining (Figure 3C, D) revealed that ISO significantly induced the formation of apoptotic bodies compared with those observed in the Con group, whereas the number of apoptotic bodies was significantly reduced in H9c2 cells treated with 15y-GP4. Flow cytometry analysis showed that exposure to ISO increased the number of cells undergoing both early and late apoptosis, whereas the number of apoptotic cells, especially late cells, was significantly reduced by the addition of 15y-GP4, suggesting that 15y-GP4 inhibited ISO-induced apoptosis (Figure 3E). Meanwhile, the addition of KC7F2 enhanced the inhibition of H9c2 apoptosis by 15y-GP4, compared with the Con sample with no interference with HIF-1α expression, whereas the addition of $CoCl_2$ reduced the inhibition of H9c2 apoptosis by 15y-GP4.

3.6 15y-GP4 treatment inhibited ISO-induced cellular ROS release

To further examine the effects of 15y-GP4 on ISO-induced ROS production in H9c2 cells, DCFH-DA was used to detect the production of ROS in ISO-induced H9c2 cells. As shown in Figure 3F, compared with the control group, the green fluorescence of H9c2 cells treated with ISO was significantly increased, indicating that ROS levels in the cells were enhanced. In contrast, green fluorescence was significantly attenuated in H9c2 cells treated with 15y-GP4, indicating that ROS levels in the cells were significantly reduced. When HIF-1α was blocked, the green fluorescence intensity was weakened compared with that of the Con cells, suggesting an increased ability of 15y-GP4 to inhibit ROS release.

3.7 15y-GP4 treatment reduced the ISO-induced mitochondrial membrane potential and inhibited the release of Ca^{2+}

In addition to being central to cellular metabolism and respiration, mitochondria also regulate intracellular Ca^{2+} concentrations. Disruption of mitochondrial function leads to a continuous inward flow of Na^+ into the cell, activating the Na^+–Ca^{2+} exchanger protein and increasing the intracellular Ca^{2+} concentration, causing intracellular calcium overload. This leads to the depolarization of the mitochondrial membrane and a reduction in membrane potential, which can result in cell death. Con cells presented predominantly red fluorescence and limited green fluorescence (Figure 3G). In contrast, ISO treatment induced a decrease in red fluorescence intensity, accompanied by a substantial increase in green fluorescence intensity. The application of 15y-GP4 to cells enhanced the red/green fluorescence ratio and increased the mitochondrial membrane potential. As shown in Figure 3H, the green fluorescence of the ISO-treated H9c2 cells was significantly enhanced. Thus, a substantial augmentation of intracellular Ca^{2+} release was observed compared with that in the Con group, whereas the intensity of green fluorescence in the cells decreased following treatment with 15y-GP4. When HIF-1α was blocked, the protective effect of 15y-GP4 on mitochondria inhibited the sustained Ca^{2+} inward flow, but activation of HIF-1α aggravated mitochondrial damage.

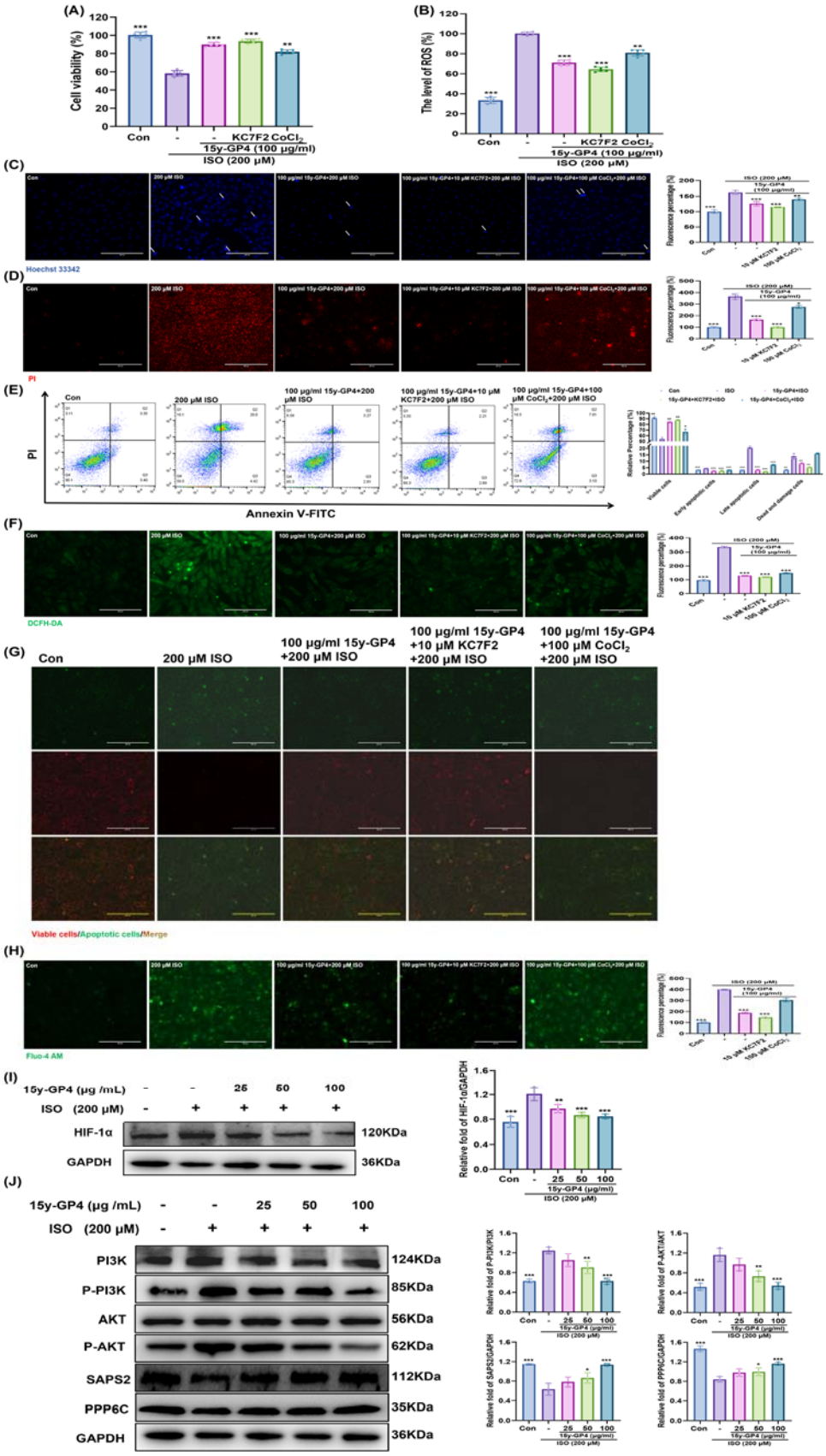

Figure. 3 Protective effect of 15y-GP4 on ISO-induced H9c2 cells. (A), Effect of hypoxia-inducible factor-1α (HIF-1α) inhibitor KC7F2 and HIF-1α activator cobalt chloride ($CoCl_2$) on cell viability in ISO-induced H9c2 cells treated with 15y-GP4. **(B)**, Effects of HIF-1α inhibitor KC7F2 and HIF-1α activator $CoCl_2$ on ROS levels in ISO-induced H9c2 cells treated with 15y-GP4. **(C)**, Hoechst 33342 staining. **(D)**, propidium iodide (PI) staining. **(E)**, Analysis of flow cytometry. **(F)**, 20,70-dichlorodihydrofluorescein diacetate (DCFH-DA) staining. **(G)**, JC-1 staining. **(H)**, Fluo-4 AM staining. **(I)**, Western blotting detection of 15y-GP4-regulated ISO-induced H9c2 cells HIF-1α expression. **(J)**, Western blotting detection of 15y-GP4-regulated ISO-induced H9c2 cells protein expression. Data are represented as mean ± SD, n=3; *$P < 0.05$, **$P < 0.01$ and ***$P < 0.001$ vs. ISO.

3.8 15y-GP4 protected cells against ISO-induced damage-related pathways

To examine the relationship between 15y-GP4 and the PI3K/Akt/HIF-1α signaling pathway, the expression of relevant proteins was determined in the Con and model groups, and in cells treated with 15y-GP4, using western blotting. As demonstrated in Figure 3I,J, the expression of p-PI3K/PI3K, p-AKT/AKT, and HIF-1α proteins were significantly increased in the model group in comparison with the Con treatment group, whereas 15y-GP4 pretreatment decreased their expression in ISO-induced H9c2 cells in a concentration-dependent manner. Activation of the PI3K/Akt/HIF-1α signaling pathway in ISO-induced H9c2 cells resulted in cell apoptosis, whereas inhibition of the PI3K/Akt/HIF-1α pathway by 15y-GP4 had a protective effect on ISO-induced H9c2 cells.

SAPS2 and PPP6C proteins were closely associated with the efficacy of 15y-GP4 in protecting against ISO-induced myocardial injury In the model group, ISO-induced H9c2 cells showed decreased intracellular expression of SAPS2 and PPP6C proteins, whereas 15y-GP4 upregulated the ISO-induced expression of SAPS2 and PPP6C proteins in the cardiomyocytes of H9c2 cells in a dose-dependent manner.

3.9 Analysis of the association between SAPS2, PPP6C, and HIF-1α protein in H9c2 cells

SAPS2-KD and PPP6C-KD engineered H9c2 cells were used to determine the role of SAPS2 and PPP6C in the cardioprotective effects of 15y-GP4. Western blotting confirmed that PPP6C and SAPS2 had been knocked down (Figure 4A, B). These findings indicated that no significant differences in enhancing cell survival or antioxidant effects of 15y-GP4 in SAPS2-KD and PPP6C-KD cell lines (Figure 4C–4F). In addition, a Co-IP assay revealed that PPP6C was associated with HIF-1α in H9c2 cells (Figure 4G). Immunofluorescence analysis confirmed the co-localization of PPP6C and HIF-1α in H9c2 cells (Figure 4H). To verify the expression of HIF-1α protein, western blotting was performed using both PPP6C-KD and SAPS2-KD cells (Figure 4I). The expression of HIF-1α protein was augmented in ISO-induced H9c2 cells within the model group. Nevertheless, 15y-GP4 did not inhibit HIF-1α protein in ISO-induced PPP6C-KD and SAPS2-KD H9c2 cells.

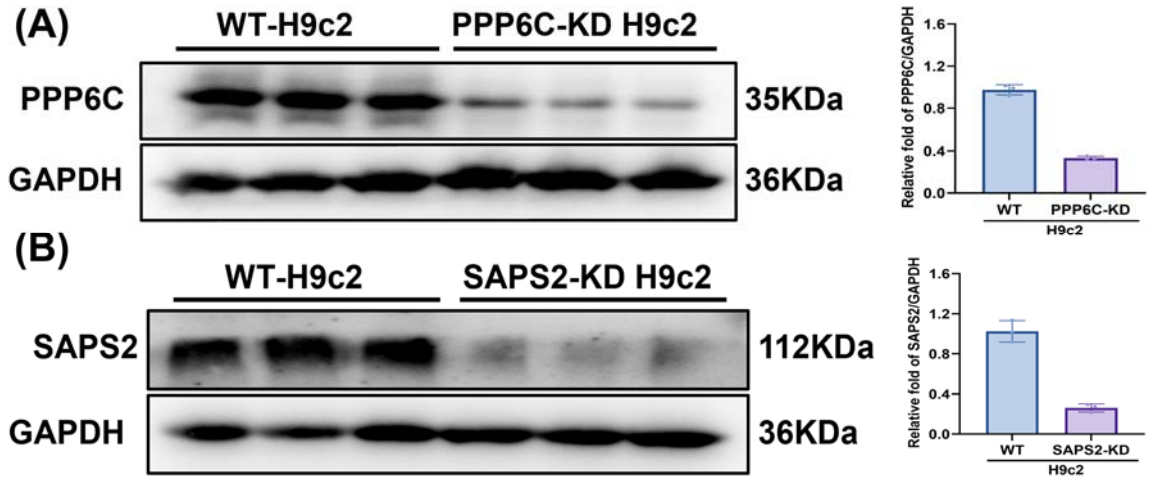

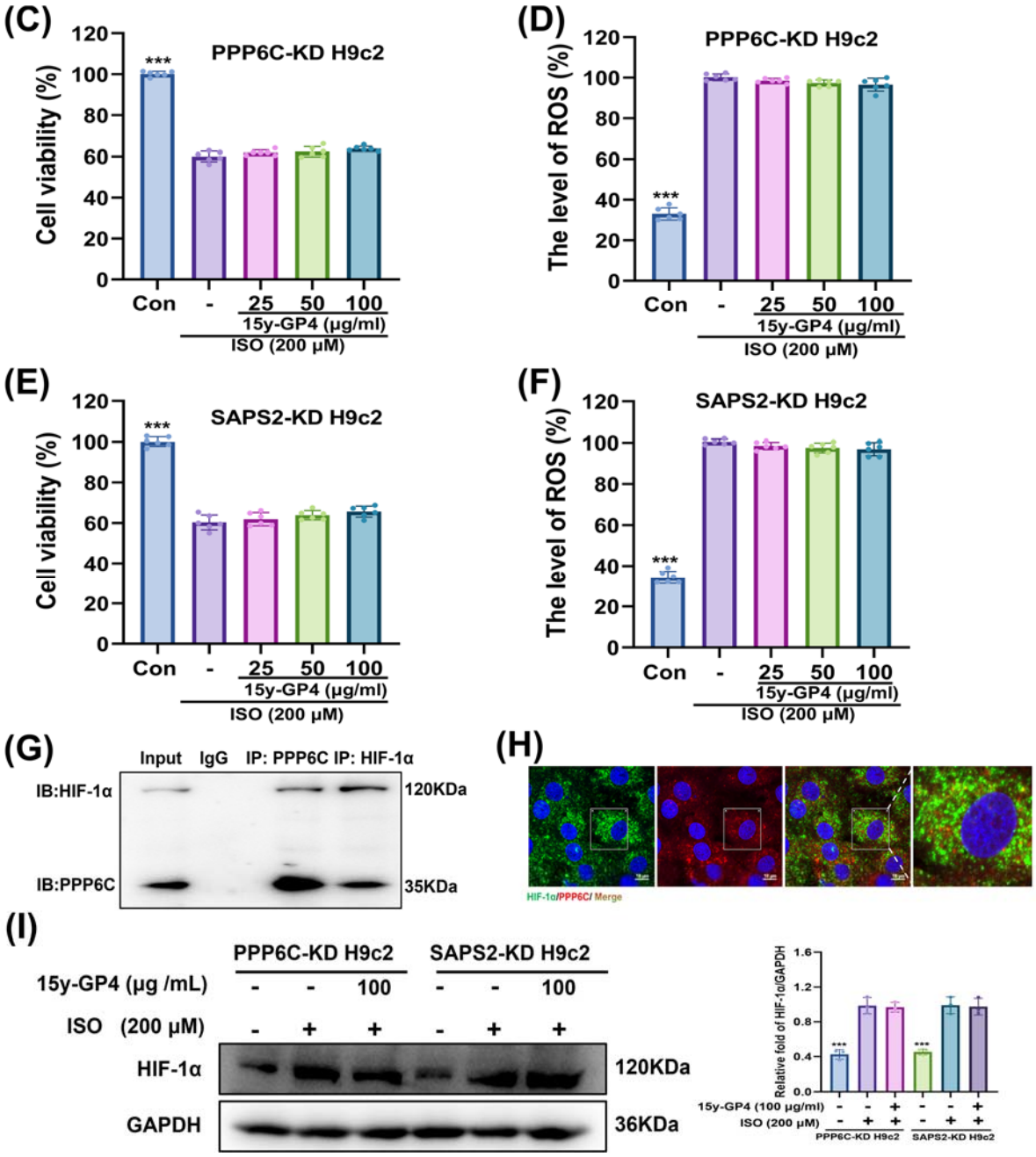

Figure. 4 Association analysis of HIF-1α protein with Protein phosphatase 6 (PP6) protein in H9C2 cells. (A), Comparison of protein phosphatase 6 catalytic subunit (PPP6C) protein expression levels between WT H9c2 and PPP6C-KD H9c2 groups. **(B)**, Comparison of phosphatase 6 regulatory subunit 2 (SAPS2) protein expression levels between WT H9c2 and SAPS2-KD H9c2 groups. **(C)**, Cell viability of 15y-GP4 in ISO-induced PPP6C-KD H9c2 cells. **(D)**, Detection of 15y-GP4 in ISO-induced PPP6C-KD H9c2 cells reactive oxygen species (ROS) level. **(E)**, Cell viability of 15y-GP4 in ISO-induced SAPS2-KD H9c2 cells. **(F)**, Detection of 15y-GP4 in ISO-induced SAPS2-KD H9c2 cells ROS level. **(G)**, Co-immunoprecipitation (Co-IP) analysis of HIF-1α protein and PPP6C protein. **(H)**, Co-localization analysis of HIF-1α protein and PPP6C protein. **(I)**, Western blotting detection of 15y-GP4-regulated ISO-induced PPP6C-KD H9c2 cells and SAPS2-KD H9c2 cells HIF-1α expression. Data are represented as mean ± SD, n=6; **P* < 0.05, ***P* < 0.01 and ****P* < 0.001 vs. ISO.

3.10 15y-GP4 alleviated ISO-induced myocardial injury in C57BL/6J mice

In this study, we evaluated the cardioprotective effects of 15y-GP4 against ISO-induced CHF in mouse models (Figure 5A). Therefore, we studied the cardiac function in mice using echocardiography (Figure 5B). The EF and FS are the most widely used clinical parameters for assessing myocardial contractility. Compared with the model group, 15y-GP4 significantly increased the EF and FS (Figure 5C, D).

Meanwhile, LVIDd and LVIDs were significantly decreased after treatment with 15y-GP4 (Figure 5E, F). Thus, 15y-GP4 increased contractility and inhibited hypertrophy in mice with ISO-induced CHF, and its therapeutic effect was stronger following 15y-GP(PM) than with 15y-GP(TM) treatment. Further evaluation of ISO-induced myocardial injury and serum levels of FFA, CK, MDA, LDH, and NT-probing revealed that the serum levels of NT-proBNP, a reliable indicator of cardiac function, were markedly increased in the model group. However, these levels were significantly suppressed by 15y-GP4 treatment (Figure 5G). In addition, 15y-GP4 significantly reduced the levels of FFA, CK, MDA, and LDH in ISO-induced CHF mice (Figure 5H-K) and inhibited HIF-1α expression (Figure 5L). ECG records the electrical activity of the heart. To test whether ISO administration in mice induced atrial fibrillation, we measured ECG signals of each ISO-treated mouse. As shown in Figure 5M, 15y-GP4 mitigated the ECG abnormalities observed in mice subjected to ISO, thereby preventing the onset of atrial fibrillation and thus, 15y-GP4 protected against myocardial injury. This conclusion is supported by the results of the histological analysis of heart tissue using H&E and Picro Sirius red trichrome staining. Cardiac tissues of mice in the model group exhibited significant tissue damage and fibrosis, and the extent of these injuries was reduced in mice treated with 15y-GP4 (Figure 5N, O). Overall, preventive treatment with 15y-GP4 significantly ameliorated myocardial damage in ISO-induced CHF mice.

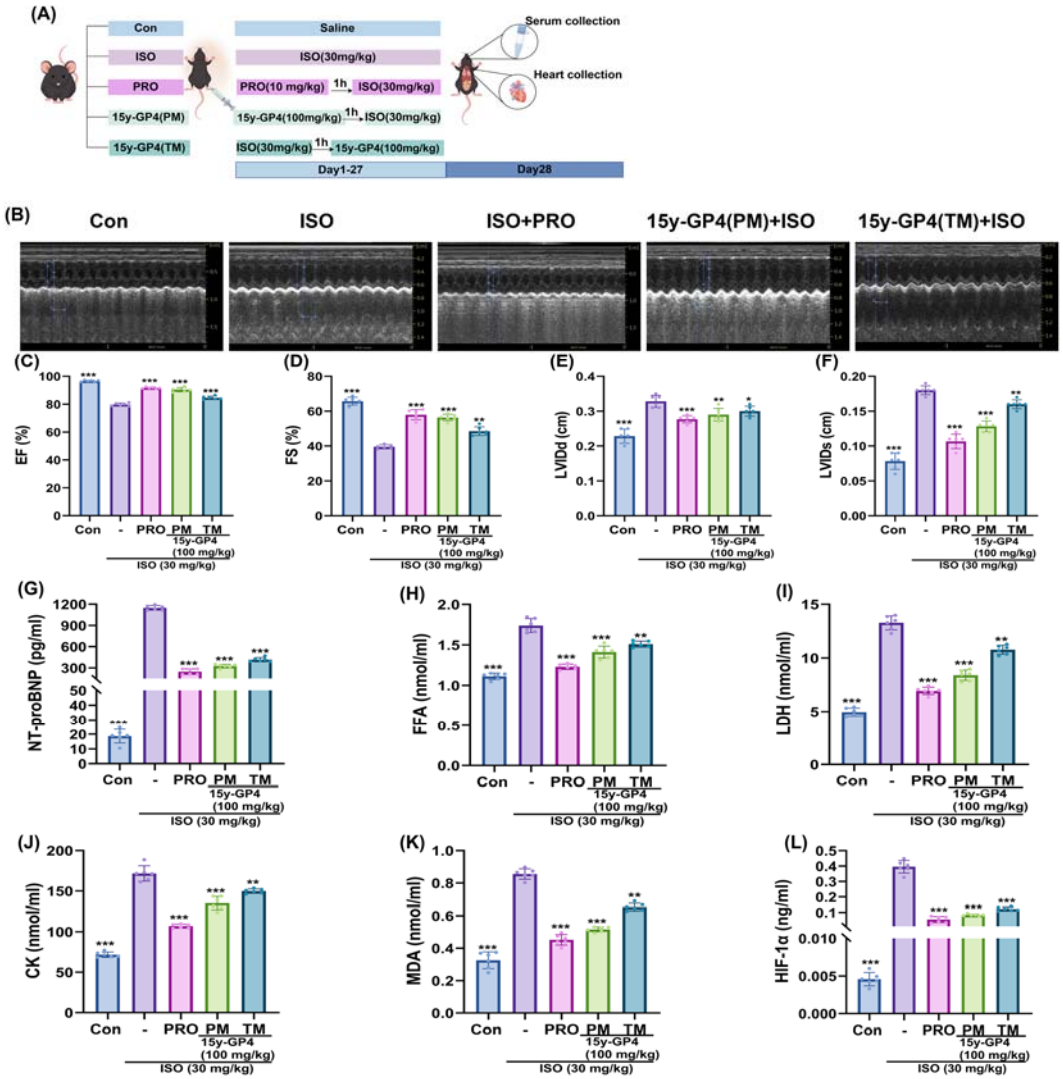

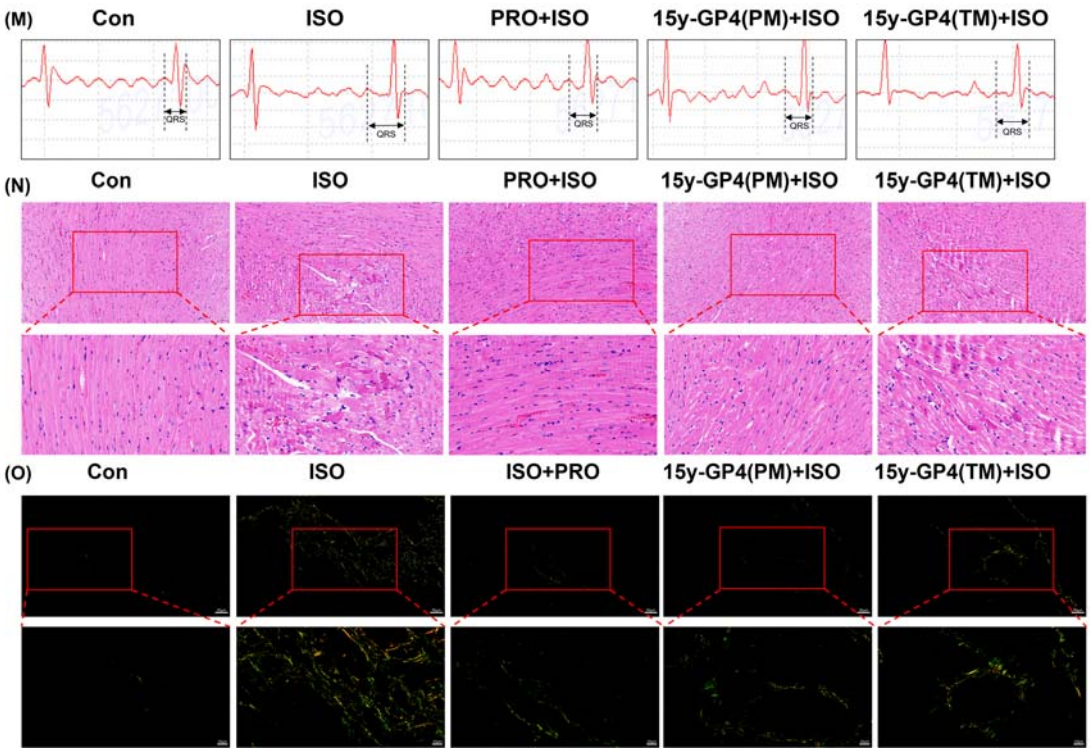

Figure. 5 Protective effect of 15y-GP4 on ISO-induced mice. (A), Flowchart of the mouse experiment. **(B)**, Echocardiography in mice. **(C)**, Analysis of ejection fraction (EF) levels in Echocardiography. **(D)**, Analysis of fractional shortening (FS) levels in Echocardiography. **(E)**, Analysis of left ventricular internal dimensions during diastole (LVIDd) levels in Echocardiography. **(F)**, Analysis of left ventricular internal dimensions during systole (LVIDs) levels in Echocardiography. **(G)**, Analysis of NT-proBNP levels in mouse serum. **(H)**, Analysis of free fatty acids (FFA) levels in mouse serum. **(I)**, Analysis of lactate dehydrogenase (LDH) levels in mouse serum. **(J)**, Analysis of creatine kinase (CK) levels in mouse serum. **(K)**, Analysis of malondialdehyde (MDA) levels in mouse serum. **(L)**, Analysis of HIF-1α levels in mouse serum. **(M)**, Electrocardiograph (ECG) in mice. **(N)**, Hematoxylin and eosin (H&E) staining. **(O)**, Picro sirius red staining. Data are represented as mean ± SD, n=6; $*P < 0.05$, $**P < 0.01$ and $***P < 0.001$ vs. ISO.

3.11 Role of HIF-1α in 15y-GP4 attenuation of ISO-induced myocardial injury in C57BL/6J mice

To further determine whether HIF-1α is associated with ISO-induced damage to the heart in mice, echocardiography was used to study cardiac function and evaluate the role of HIF-1α in the cardioprotective effects of 15y-GP4 in ISO-induced CHF mice (Figure 6A). The concomitant use of KC7F2 and 15y-GP4 increased EF and FS and led to a decrease in LVIDd and LVIDs compared with mice that received only 15y-GP4 treatment; the use of $CoCl_2$ diminished the therapeutic effects of 15y-GP4 (Figure 6B-E). The ability of 15y-GP4 to reduce FFA, CK, MDA, and LDH levels in ISO-induced CHF mice was enhanced when HIF-1α expression was inhibited (Figure 6F–K). Western blotting demonstrated that 15y-GP4 could exert a protective effect against cardiac injury in mice by inhibiting HIF-1α expression. When HIF-1α expression was inhibited, the expression of PPP6C and SAPS2 increased (Figure 6L). Electrocardiograms showed that inhibiting HIF-1α expression augmented the effectiveness of 15y-GP4 in impeding the development of atrial fibrillation (Figure 6M). Furthermore, H&E and Picro Sirius red staining of heart samples revealed that suppression of HIF-1α expression enhanced the protective efficacy of 15y-GP4 in mitigating myocardial injury (Figure 6N,O). Overall, the findings indicated that elevated levels of HIF-1α amplify the severity of ISO-induced cardiac injury in CHF model mice. Furthermore, 15y-GP4 can attenuate ISO-induced cardiac injury by modulating HIF-1α expression.

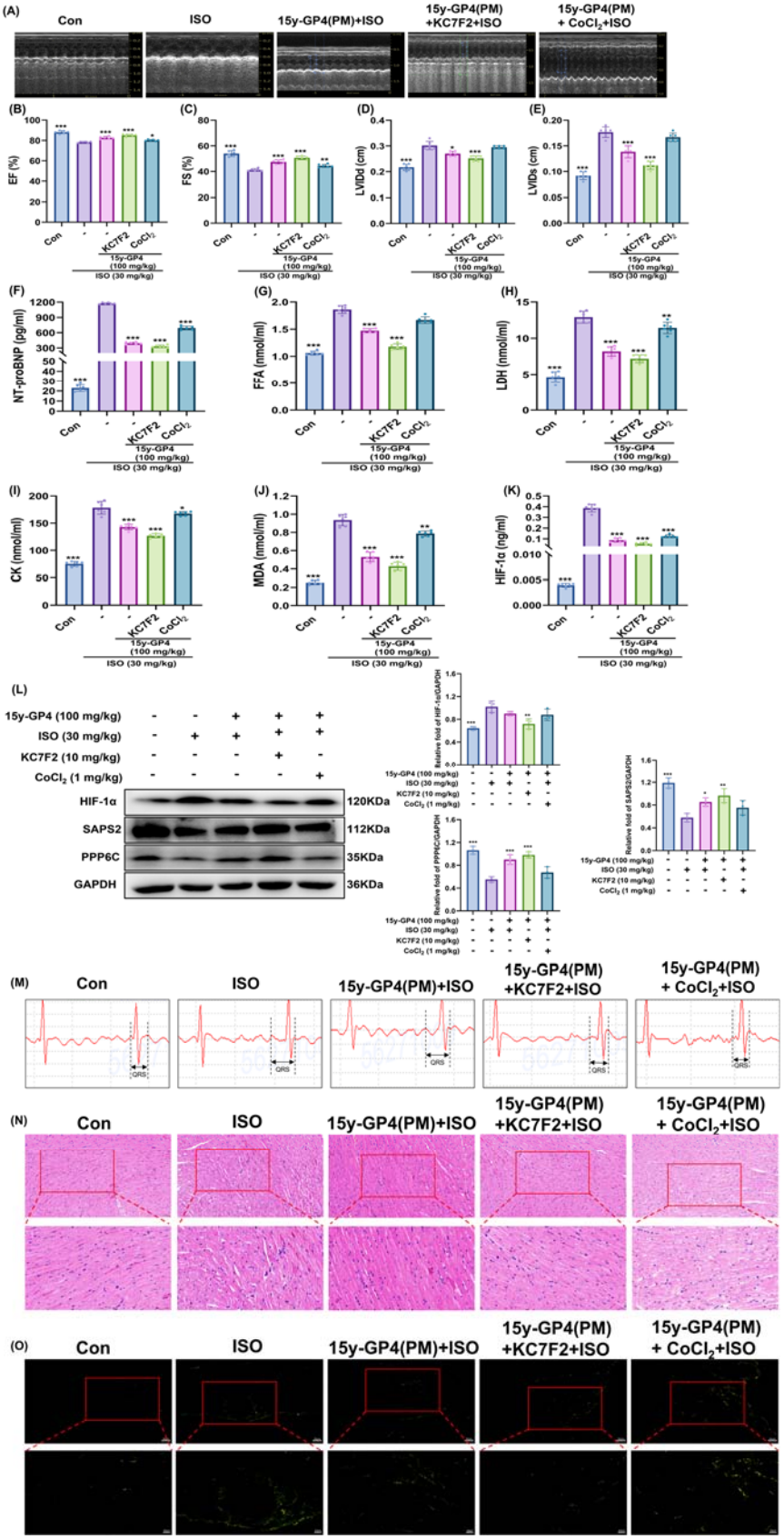

Figure. 6 Role of HIF-1α protein in 15y-GP4 protection of ISO-induced mice. (A), Echocardiography in mice. **(B)**, Analysis of EF levels in Echocardiography. **(C)**, Analysis of FS levels in Echocardiography. **(D)**, Analysis of LVIDd levels in Echocardiography. **(E)**, Analysis of LVIDs levels in Echocardiography. **(F)**, Analysis of NT-proBNP levels in mouse serum. **(G)**, Analysis of FFA levels in mouse serum. **(H)**, Analysis of LDH levels in mouse serum. **(I)**, Analysis of CK levels in mouse serum. **(J)**, Analysis of MDA levels in mouse serum. **(K)**, Analysis of HIF-1α levels in mouse serum. **(L)**, Effects of HIF-1α inhibitor KC7F2 and HIF-1α activator $CoCl_2$ on HIF-1α protein levels in ISO-induced mouse tissue treated with 15y-GP4. **(M)**, ECG in mice. **(N)**, H&E staining. **(O)**, Picro sirius red staining. Data are represented as mean ± SD, n=6; *P < 0.05, **P < 0.01 and ***P < 0.001 vs. ISO.

In summary, 15y-GP4 exerted a therapeutic effect on CHF by targeting the PI3K/AKT/HIF-1α axis and acting as an antioxidant (Figure 7).

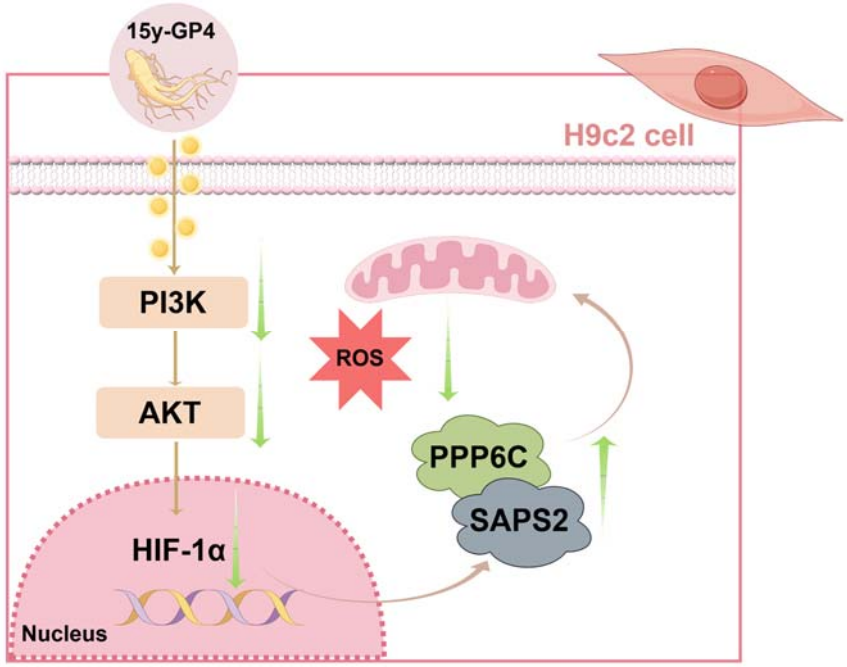

Figure. 7 15y-GP4 cardioprotective mechanism diagram.

4. Discussion

CHF is a progressive disease wherein the heart is unable to provide sufficient energy to meet metabolic demands. A reduction in the supply of energy because of hypoxia and subsequent mitochondrial dysfunction has a significant impact on the metabolism of cardiomyocytes, thereby impairing their function [25]. The pathogenesis of CHF involves multiple factors including oxidative stress, cardiomyocyte apoptosis, calcium overload, and mitochondrial dysfunction [26, 27]. Oxidative str<ess, a key pathogenic mechanism of mitochondrial dysfunction, plays an important role as a driving force in the onset and progression of CHF, and treatment of mitochondrial damage is necessary for maintaining cardiac homeostasis [28]. Furthermore, increased ROS production can have a devastating effect on cellular function and integrity, and may ultimately trigger cardiomyocyte apoptosis [29].

HIF-1α is a pivotal transcription factor in the adaptive hypoxic response. Prolonged upregulation of HIF-1α has been demonstrated to have deleterious effects on cardiac function [30]. Cardiac-specific VHL knockout mice models present spontaneous cardiac dysfunction and the sustained expression of HIF-1α inhibits the oxidation of fatty acids and increases the synthesis of triacylglycerol. This leads to lipid accumulation and apoptosis in heart muscle cells, which in turn induce cardiac hypertrophy, myocardial fibrosis, and CHF [31, 32]. Dysregulation of HIF-1α is therefore associated with different cardiac illnesses. Most studies suggest that this response is distinct from the adaptive reaction to acute injury. The prolonged activation of PI3K/AKT signaling promotes oxidative stress and mitochondrial damage in cardiomyocytes [33, 34], while long-term sustained upregulation of the PI3K/Akt pathway promotes apoptosis and causes structural damage to the myocardium [35]. The PI3K/AKT signaling pathway has been shown to regulate

cardiac function through modulation of HIF-1α protein expression [36]. This mechanism aligns with the role of HIF-1α in regulating mitochondrial biogenesis and oxidative stress under hypoxic conditions, where HIF-1α stabilization exacerbates mitochondrial damage by promoting excessive ROS production and impairing electron transport chain efficiency. By inhibiting the PI3K/Akt/HIF-1α axis, excessive mitochondrial fission can be improved, restoring the dynamic balance between mitochondrial fission and fusion [37, 38].

In this study, ISO was selected as the inducer of CHF in mouse models. ISO is a non-selective β-AR agonist. Excessive heart rate acceleration increases the myocardial burden and exacerbates the mismatch between oxygen supply; this can cause chronic activation of the hypoxic response of the heart, ultimately leading to pathologic fibrosis and disruption of myocardial structure and function, which in turn can potentially trigger CHF [39]. Vanillin has been reported to prevent ISO-induced myocardial injury by modulating the Akt/HIF-1α/VEGF signaling pathway[40]. Although beta-blockers continue to be an important part of the current treatment of CHF, they have several limitations [41]. Therefore, to address this clinical need, it is imperative to achieve a comprehensive understanding regarding CHF and identify novel therapeutic targets.

To study the function of HIF-1α in ISO-induced CHF, the HIF-1α inducer $CoCl_2$ and the inhibitor KC7F2 were utilized to intervene in cellular and mouse models, respectively. We systematically assessed the effects of 15y-GP on the preventive effect of CHF by modulating the expression of HIF-1α. This experimental design identified a key role for HIF-1α in the development of CHF and provided an important basis for exploring the cardioprotective mechanism of GP. Specifically, $CoCl_2$ is recognized as an active inducer of HIF-1α and can stabilize the protein and prevent its degradation under non-monomorphic conditions, thus promoting the accumulation and nucleation of HIF-1α and enhancing its transcriptional activity [42]. At cellular and animal levels, $CoCl_2$ treatment significantly upregulates HIF-1α protein expression[43]. KC7F2 is a small molecule featuring a cysteamine core structure. KC7F2 can inhibit HIF-1α translation and has been shown to inhibit HIF-1α transcription; therefore, KC7F2 is a commonly used HIF-1α inhibitor [44]. We showed that ISO treatment resulted in high HIF-1α expression, leading to cardiac fibrosis and CHF. The results also showed that these changes were related to HIF-1α-mediated mitochondrial damage and cardiomyocyte apoptosis. Both *in vitro* and *in vivo* experiments using $CoCl_2$ and KC7F2 highlighted an interesting point: when $CoCl_2$ was used to induce high levels of HIF-1α expression, the CHF preventive effect of 15y-GP4 was attenuated, cardiac function deteriorated, and arrhythmias worsened compared to the 15y-GP4(PM) group. In contrast, treatment with the HIF-1α inhibitor KC7F2 further increased the ability of 15y-GP4 to attenuate oxidative stress injury, improve mitochondrial function, and reduce cardiomyocyte apoptosis. Thus, 15y-GP4 prevented CHF by protecting cardiomyocytes from oxidative stress injury through inhibition of HIF-1α. These findings not only confirmed the key regulatory role of HIF-1α in ISO-induced CHF but also revealed that the cardioprotective mechanism of 15y-GP4 may

be achieved by inhibiting the HIF-1α signaling pathway, thus providing a new theoretical basis for targeted therapy of CHF.

The marked anti-apoptotic and antioxidant properties of ginseng have been previously described [45]. Oxidative stress and apoptosis are two important phenomena of CHF pathology [46, 47]. We observed that the cardioprotective effects of GP derived from ginseng samples increased with ageing. We extracted and screened an acidic heteropolysaccharide from 15y-GP and found that it was primarily composed of Glc monosaccharides. The antioxidant properties of polysaccharides are associated with their structural characteristics, including chain configuration, molecular structure, and monosaccharide composition. These factors collectively influence the activity of polysaccharides.

PP6, a key serine/threonine phosphatase, exhibits a unique heterotrimeric structure in which the catalytic subunit PPP6C and regulatory subunit SAPS2 play critical roles [21]. PP6 expression is widespread in cells; as a key intracellular signaling regulatory molecule, PP6 controls a broad spectrum of physiological processes, including several crucial inflammatory responses, autophagy, and neurite growth. PP6 is abundantly expressed in heart and skeletal muscles, highlighting its important roles in these tissues [48]. Genome-wide screening studies have revealed that PP6 is a key negative regulator of apoptosis. In the present study, ISO treatment suppressed SAPS2 and PPP6C expression, whereas ginseng treatment increased SAPS2 and PPP6C expression. SAPS2 and PPP6C have been recognized as potential key targets for myocardial function. Here, we correlated HIF-1α with PPP6 and propose, for the first time, that GP prevents ISO-induced myocardial injury through the PI3K/AKT/HIF-1α pathway as well as through the interaction of SAPS2, PPP6C, and HIF-1α.

This study revealed the mechanisms underlying the cardioprotective effects of the GP fraction 15y-GP4. We showed that 15y-GP4 significantly suppressed ISO-induced HIF-1α overexpression by inhibiting the PI3K/AKT signaling pathway. HIF-1α can interact with PPP6 protein to co-regulate the level of oxidative stress and apoptotic processes of cardiomyocytes. Meanwhile, specific inhibition of HIF-1α expression can significantly ameliorate ISO-induced cardiomyocyte injury, thus effectively reducing cardiac tissue injury. These findings not only confirm the importance of HIF-1α as a key target for CHF treatment at the molecular level but also indicate that GP, as a natural HIF-1α modulator, can facilitate the prevention of CHF as well as the development of a novel strategy for adjuvant therapy in patients with CHF.

This study identifies candidate drugs for long-term chronic administration in patients with CHF and offers a rationale for the development of polysaccharide-based cardioprotective agents. Nonetheless, it should be considered that etiologies of CHF in clinical settings are diverse, and as our findings were based solely on an ISO-induced CHF model, these may not be generalizable to a broader CHF population. In the future, we plan to validate these findings using multiple CHF models.

5. Conclusion

This study revealed that CHF in mice is associated with upregulated HIF-1α and downregulated PPP6 expression. We demonstrated that the ginseng polysaccharide derivative 15y-GP4 alleviates ISO-induced

CHF by inhibiting the HIF-1α signaling pathway. This treatment improved mitochondrial function, reduced oxidative stress, and suppressed cardiomyocyte apoptosis, effectively attenuating cardiac structural damage and fibrosis. These results suggest that 15y-GP4 is a promising candidate for future drug development and underscores the potential of 15-year-old-ginseng as a high-value industrial crop for cardiovascular therapy.

Funding

This work was supported by the National Natural Science Foundation of China (Grant No. 82204719); Natural Science Foundation for Excellent Young Scholars of Jilin Province of China (Grant No. 20250101053JJ); Science Fund for Distinguished Young Scholars of CCUCM (Grant No. 2024JQ06).

Declaration of Competing Interest

The authors declare that they have no known competing financial interests or personal relationships that could have appeared to influence the work reported in this paper.

Data availability

Data will be made available on request.

References

[1] T. Xu, Y. Wan, J. Zhang, et al., Why ginseng has protective functions on the heart, European journal of preventive cardiology. 25 (2018) 1150-1151. https://doi.org/10.1177/2047487318768943.

[2] J.-E. Han, H.-S. Lee, E.-J. Son, et al., Changes in the dynamic profile of beneficial metabolites during Panax ginseng somatic embryogenesis, Industrial Crops and Products. 234 (2025) https://doi.org/10.1016/j.indcrop.2025.121535.

[3] Z. Zhou, M. Li, Z. Zhang, et al., Overview of Panax ginseng and its active ingredients protective mechanism on cardiovascular diseases, Journal of ethnopharmacology. 334 (2024) 118506. https://doi.org/10.1016/j.jep.2024.118506.

[4] J.H. Lee, D.H. Kim, M. Kim, et al., Mitochondrial ROS-Mediated Metabolic and Cytotoxic Effects of Isoproterenol on Cardiomyocytes Are p53-Dependent and Reversed by Curcumin, Molecules. 27 (2022) https://doi.org/10.3390/molecules27041346.

[5] Z. Liu, X. Bian, W. Gao, et al., Rg3 promotes the SUMOylation of SERCA2a and corrects cardiac dysfunction in heart failure, Pharmacol Res. 172 (2021) 105843. https://doi.org/10.1016/j.phrs.2021.105843.

[6] S. Wan, Z. Cui, L. Wu, et al., Ginsenoside Rd promotes omentin secretion in adipose through TBK1-AMPK to improve mitochondrial biogenesis via WNT5A/Ca(2+) pathways in heart failure, Redox Biol. 60 (2023) 102610. https://doi.org/10.1016/j.redox.2023.102610.

[7] Y.H. Zuo, Q.B. Han, G.T. Dong, et al., Panax ginseng Polysaccharide Protected H9c2 Cardiomyocyte From Hypoxia/Reoxygenation Injury Through Regulating Mitochondrial Metabolism and RISK Pathway, Frontiers in physiology. 9 (2018) 699. https://doi.org/10.3389/fphys.2018.00699.

[8] M. Jiang, X. Fan, Y. Wang, et al., Effects of hypoxia in cardiac metabolic remodeling and heart failure, Experimental cell research. 432 (2023) 113763. https://doi.org/10.1016/j.yexcr.2023.113763.

[9] B. Zhou, R. Tian, Mitochondrial dysfunction in pathophysiology of heart failure, The Journal of clinical investigation. 128 (2018) 3716-3726. https://doi.org/10.1172/jci120849.

[10] H. Zhu, Q. Jin, Y. Li, et al., Melatonin protected cardiac microvascular endothelial cells against oxidative stress injury via suppression of IP3R-[Ca(2+)]c/VDAC-[Ca(2+)]m axis by activation of MAPK/ERK signaling pathway, Cell stress & chaperones. 23 (2018) 101-113. https://doi.org/10.1007/s12192-017-0827-4.

[11] Q. Jin, R. Li, N. Hu, et al., DUSP1 alleviates cardiac ischemia/reperfusion injury by suppressing the Mff-required mitochondrial fission and Bnip3-related mitophagy via the JNK pathways, Redox Biol. 14 (2018) 576-587. https://doi.org/10.1016/j.redox.2017.11.004.

[12] H. Zhou, S. Wang, P. Zhu, et al., Empagliflozin rescues diabetic myocardial microvascular injury via AMPK-mediated inhibition of mitochondrial fission, Redox Biol. 15 (2018) 335-346. https://doi.org/10.1016/j.redox.2017.12.019.

[13] P. Zhu, S. Hu, Q. Jin, et al., Ripk3 promotes ER stress-induced necroptosis in cardiac IR injury: A mechanism involving calcium overload/XO/ROS/mPTP pathway, Redox Biol. 16 (2018) 157-168. https://doi.org/10.1016/j.redox.2018.02.019.

[14] N. Buijs, J.E. Oosterink, M. Jessup, et al., A new key player in VEGF-dependent angiogenesis in human hepatocellular carcinoma: dimethylarginine dimethylaminohydrolase 1, Angiogenesis. 20 (2017) 557-565. https://doi.org/10.1007/s10456-017-9567-4.

[15] Q.Q. Cheng, Y.W. Wan, W.M. Yang, et al., Gastrodin protects H9c2 cardiomyocytes against oxidative injury by ameliorating imbalanced mitochondrial dynamics and mitochondrial dysfunction, Acta Pharmacol Sin. 41 (2020) 1314-1327. https://doi.org/10.1038/s41401-020-0382-x.

[16] C.J. Schofield, P.J. Ratcliffe, Oxygen sensing by HIF hydroxylases, Nature reviews. Molecular cell biology. 5 (2004) 343-354. https://doi.org/10.1038/nrm1366.

[17] Y.J. Zhang, X.L. Zhang, M.H. Li, et al., The ginsenoside Rg1 prevents transverse aortic constriction-induced left ventricular hypertrophy and cardiac dysfunction by inhibiting fibrosis and enhancing angiogenesis, Journal of cardiovascular pharmacology. 62 (2013) 50-57. https://doi.org/10.1097/FJC.0b013e31828f8d45.

[18] K. Yang, P. Zhang, J. Li, et al., Potential of natural drug modulation of endoplasmic reticulum stress in the treatment of myocardial injury, Journal of pharmaceutical analysis. 14 (2024) 101034. https://doi.org/10.1016/j.jpha.2024.101034.

[19] M. Hölscher, K. Schäfer, S. Krull, et al., Unfavourable consequences of chronic cardiac HIF-1α stabilization, Cardiovascular research. 94 (2012) 77-86. https://doi.org/10.1093/cvr/cvs014.

[20] Z. Zhang, L. Yao, J. Yang, et al., PI3K/Akt and HIF-1 signaling pathway in hypoxia-ischemia (Review), Molecular medicine reports. 18 (2018) 3547-3554. https://doi.org/10.3892/mmr.2018.9375.

[21] N. Kitamura, T. Ohama, K. Sato, Protein phosphatase 6 promotes transforming growth factor-β signaling in mouse embryonic fibroblasts, The Journal of veterinary medical science. 85 (2023) 1319-1323. https://doi.org/10.1292/jvms.23-0380.

[22] Q. Li, Y. Xie, Z. Cui, et al., Activation of hypoxia-inducible factor 1 (Hif-1) enhanced bactericidal effects of macrophages to Mycobacterium tuberculosis, Tuberculosis (Edinburgh, Scotland). 126 (2021) 102044. https://doi.org/10.1016/j.tube.2020.102044.

[23] J.F. Qian, S.Q. Liang, Q.Y. Wang, et al., Isoproterenol induces MD2 activation by β-AR-cAMP-PKA-ROS signalling axis in cardiomyocytes and macrophages drives inflammatory heart failure, Acta Pharmacol Sin. 45 (2024) 531-544. https://doi.org/10.1038/s41401-023-01179-3.

[24] J. Wu, L. Yang, P. Xie, et al., Cobalt Chloride Upregulates Impaired HIF-1α Expression to Restore Sevoflurane Post-conditioning-Dependent Myocardial Protection in Diabetic Rats, Frontiers in physiology. 8 (2017) 395. https://doi.org/10.3389/fphys.2017.00395.

[25] T. Sato, N. Takeda, The roles of HIF-1α signaling in cardiovascular diseases, Journal of cardiology. 81 (2023) 202-208. https://doi.org/10.1016/j.jjcc.2022.09.002.

[26] T. Zhang, L. Li, X. Mo, et al., Matairesinol blunts adverse cardiac remodeling and heart failure induced by pressure overload by regulating Prdx1 and PI3K/AKT/FOXO1 signaling, Phytomedicine. 135 (2024) 156054. https://doi.org/10.1016/j.phymed.2024.156054.

[27] B.S. Karam, A. Chavez-Moreno, W. Koh, et al., Oxidative stress and inflammation as central mediators of atrial fibrillation in obesity and diabetes, Cardiovascular diabetology. 16 (2017) 120. https://doi.org/10.1186/s12933-017-0604-9.

[28] J. Fu, C. Su, Y. Ge, et al., PDE4D inhibition ameliorates cardiac hypertrophy and heart failure by activating mitophagy, Redox Biol. 81 (2025) 103563. https://doi.org/10.1016/j.redox.2025.103563.

[29] M. Liu, G. Galli, Y. Wang, et al., Novel Therapeutic Targets for Hypoxia-Related Cardiovascular Diseases: The Role of HIF-1, Frontiers in physiology. 11 (2020) 774. https://doi.org/10.3389/fphys.2020.00774.

[30] P.G. Sant'Ana, L.C. Tomasi, G.M. Murata, et al., Hypoxia-Inducible Factor 1-Alpha and Glucose Metabolism during Cardiac Remodeling Progression from Hypertrophy to Heart Failure, Int J Mol Sci. 24 (2023) https://doi.org/10.3390/ijms24076201.

[31] B. Yu, X. Wang, Y. Song, et al., The role of hypoxia-inducible factors in cardiovascular diseases, Pharmacology & therapeutics. 238 (2022) 108186. https://doi.org/10.1016/j.pharmthera.2022.108186.

[32] Y. Zhou, K. Song, B. Tu, et al., METTL3 boosts glycolysis and cardiac fibroblast proliferation by increasing AR methylation, International journal of biological macromolecules. 223 (2022) 899-915. https://doi.org/10.1016/j.ijbiomac.2022.11.042.

[33] N. Zhu, T. Li, Y. Bai, et al., Targeting myocardial inflammation: investigating the therapeutic potential of atrial natriuretic peptide in atrial fibrosis, Molecular biology reports. 51 (2024) 506. https://doi.org/10.1007/s11033-024-09393-w.

[34] W.W. Zhou, C. Dai, W.Z. Liu, et al., Gentianella acuta improves TAC-induced cardiac remodelling by regulating the Notch and PI3K/Akt/FOXO1/3 pathways, Biomedicine & pharmacotherapy = Biomedecine & pharmacotherapie. 154 (2022) 113564. https://doi.org/10.1016/j.biopha.2022.113564.

[35] M. Packer, Qiliqiangxin: A multifaceted holistic treatment for heart failure or a pharmacological probe for the identification of cardioprotective mechanisms?, European journal of heart failure. 25 (2023) 2130-2143. https://doi.org/10.1002/ejhf.3068.

[36] X. Li, Z. Gui, H. Liu, et al., Remifentanil pretreatment ameliorates H/R-induced cardiac microvascular endothelial cell dysfunction by regulating the PI3K/Akt/HIF-1α signaling pathway, Bioengineered. 12 (2021) 7872-7881. https://doi.org/10.1080/21655979.2021.1969843.

[37] J. Wang, H. Zhuang, C. Li, et al., Ligustrazine nano-drug delivery system ameliorates doxorubicin-mediated myocardial injury via piezo-type mechanosensitive ion channel component 1-prohibitin 2-mediated mitochondrial quality surveillance, Journal of nanobiotechnology. 23 (2025) 383. https://doi.org/10.1186/s12951-025-03420-z.

[38] X. Pu, J. Liu, Y. Wang, et al., Ginsenoside Rb1 attenuates coronary microvascular inflammatory injury via NDUFS4-SIRT5-DUSP1-mediated mitochondrial quality control in a murine ischemia-reperfusion model, Journal of ginseng research. 49 (2025) 509-522. https://doi.org/10.1016/j.jgr.2025.04.006.

[39] N. Keaney, Isoprenaline and practolol, Lancet (London, England). 1 (1970) 306-307. https://doi.org/10.1016/s0140-6736(70)90678-1.

[40] M.M. Elseweidy, S.I. Ali, M.A. Shaheen, et al., Vanillin and pentoxifylline ameliorate isoproterenol-induced myocardial injury in rats via the Akt/HIF-1α/VEGF signaling pathway, Food Funct. 14 (2023) 3067-3082. https://doi.org/10.1039/d2fo03570g.

[41] J. Xu, S. Liang, Q. Wang, et al., JOSD2 mediates isoprenaline-induced heart failure by deubiquitinating CaMKIIδ in cardiomyocytes, Cellular and molecular life sciences : CMLS. 81 (2024) 18. https://doi.org/10.1007/s00018-023-05037-7.

[42] Z.J. Dai, J. Gao, X.B. Ma, et al., Up-regulation of hypoxia inducible factor-1α by cobalt chloride correlates with proliferation and apoptosis in PC-2 cells, Journal of experimental & clinical cancer research : CR. 31 (2012) 28. https://doi.org/10.1186/1756-9966-31-28.

[43] P. Wang, G. Zeng, Y. Yan, et al., Disruption of adipocyte HIF-1α improves atherosclerosis through the inhibition of ceramide generation, Acta pharmaceutica Sinica. B. 12 (2022) 1899-1912. https://doi.org/10.1016/j.apsb.2021.10.001.

[44] T. Narita, S. Yin, C.F. Gelin, et al., Identification of a novel small molecule HIF-1alpha translation inhibitor, Clinical cancer research : an official journal of the American Association for Cancer Research. 15 (2009) 6128-6136. https://doi.org/10.1158/1078-0432.Ccr-08-3180.

[45] S. Liu, J. Geng, W. Chen, et al., Isolation, structure, biological activity and application progress of ginseng polysaccharides from the Araliaceae family, International journal of biological macromolecules. 276 (2024) 133925. https://doi.org/10.1016/j.ijbiomac.2024.133925.

[46] L. Xing, Y. Liu, J. Wang, et al., High-Density Lipoprotein and Heart Failure, Reviews in cardiovascular medicine. 24 (2023) 321. https://doi.org/10.31083/j.rcm2411321.

[47] L. Si, Y. Lai, Pharmacological mechanisms by which baicalin ameliorates cardiovascular disease, Front Pharmacol. 15 (2024) 1415971. https://doi.org/10.3389/fphar.2024.1415971.

[48] H. Bastians, H. Ponstingl, The novel human protein serine/threonine phosphatase 6 is a functional homologue of budding yeast Sit4p and fission yeast ppe1, which are involved in cell cycle regulation, Journal of cell science. 109 (Pt 12) (1996) 2865-2874. https://doi.org/10.1242/jcs.109.12.2865.